SUPPLEMENTARY INFORMATION

Structure of human ferroportin reveals molecular basis of iron homeostasis

Christian B. Billesboelle[1]*, Caleigh M. Azumaya[2]*, Rachael C. Kretsch[3-7], Alex S. Powers[3-7], Shane Gonen[2,8,9], Simon Schneider[10], Tara Arvedson[11], Ron O. Dror[3-7], Yifan Cheng[2,8], Aashish Manglik[1,2]

[1]Department of Pharmaceutical Chemistry, University of California, San Francisco, 1700 4th Street, San Francisco, CA 94158, USA.
[2]Department of Biochemistry and Biophysics, University of California, San Francisco, 600 16th Street, San Francisco, CA 94158, USA.
[3]Department of Molecular and Cellular Physiology, Stanford University School of Medicine, Stanford, CA 94305, USA
[4]Department of Structural Biology, Stanford University School of Medicine, Stanford, CA 94305, USA
[5]Department of Computer Science, Stanford University, Stanford, CA 94305, USA
[6]Institute for Computational and Mathematical Engineering, Stanford University, Stanford, CA 94305, USA
[7]Biophysics Program, Stanford University, Stanford, CA 94305, USA
[8]Howard Hughes Medical Institute, University of California San Francisco, San Francisco, CA, USA
[9]Present address: Department of Molecular Biology and Biochemistry, University of California, Irvine, 2224 Biological Sciences III, Irvine, CA 92697, USA
[10]Institute of Biochemistry, Goethe University Frankfurt, Max-von-Laue-Straße 9, 60438 Frankfurt am Main, Germany
[11]Department of Oncology Research, Amgen Inc., South San Francisco, CA, United States
[12]Department of Anesthesia and Perioperative Care, University of California, San Francisco, 1700 4th Street, San Francisco, CA 94158, USA.

* These authors contributed equally
Correspondence to Yifan Cheng (Yifan.Cheng@ucsf.edu) or Aashish Manglik (Aashish.Manglik@ucsf.edu)

SUPPLEMENTARY FIGURES

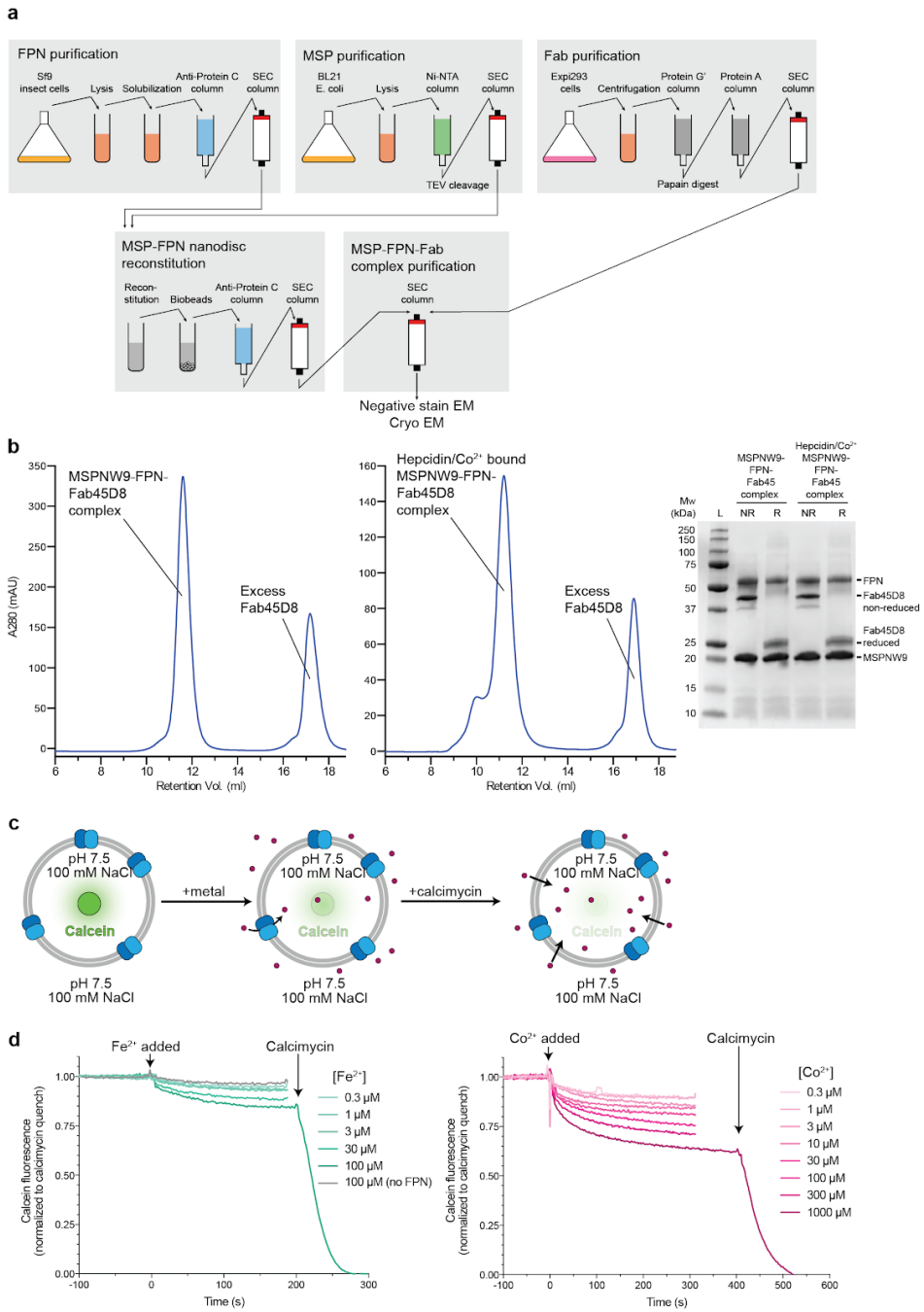

Supplementary Figure 1. Biochemistry of purified human ferroportin. a, Purification scheme for nanodisc-reconstituted FPN bound to Fab45D8 for cryo-EM studies. **b,** Size exclusion chromatography of purified apo and hepcidin/Co^{2+} bound FPN-Fab45D8 complex. SDS-PAGE gel of purified complex under non-reducing (NR) and reducing (R) conditions. **c,** Schematic of calcein-based assay to measure transport of divalent cations. Purified FPN is reconstituted into proteoliposomes containing calcein. Addition of divalent cations leads to quenching of calcein fluorescence. Addition of the divalent cation ionophore calcimycin fully quenches calcein fluorescence. **d,** Reconstituted human FPN transports Fe^{2+} and Co^{2+}.

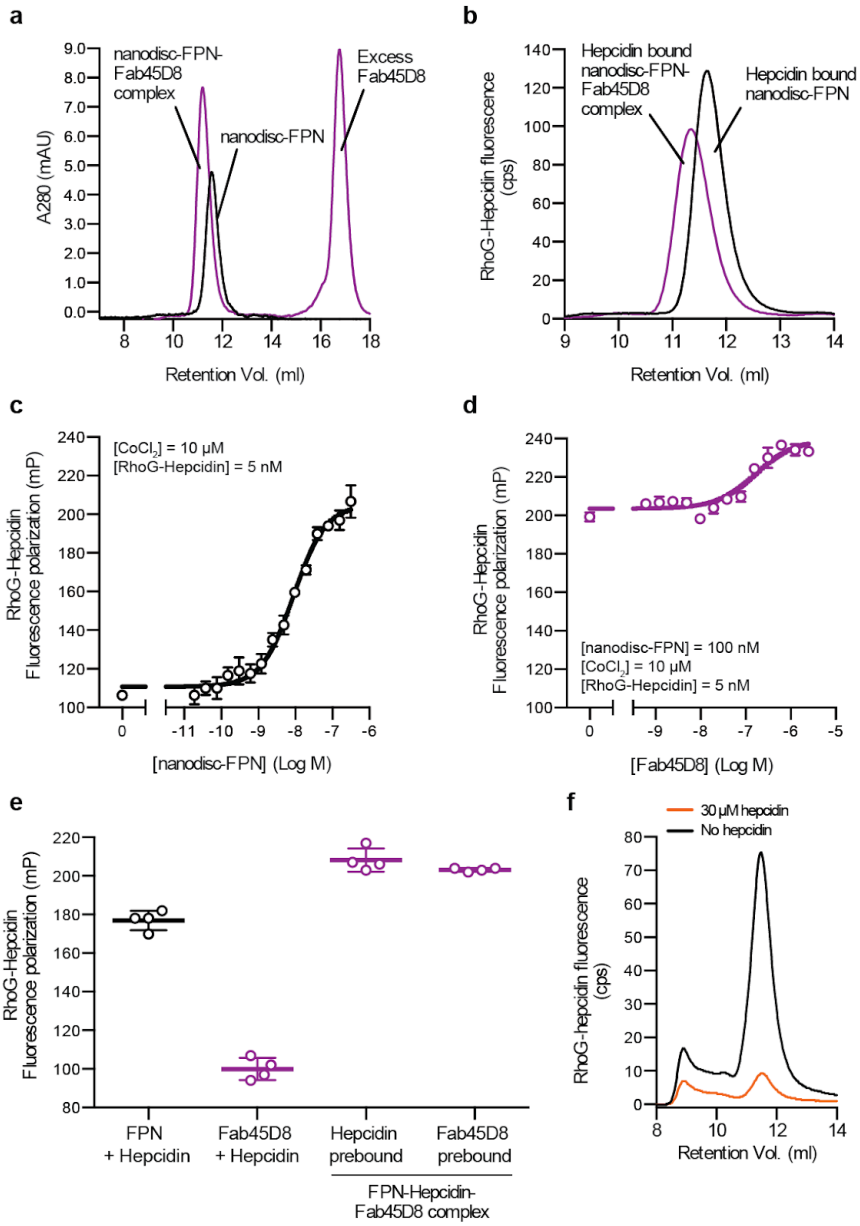

Supplementary Figure 2. Characterization of Fab45D8. a, Fab45D8 binds nanodisc-reconstituted FPN (nanodisc-FPN), as assessed by size-exclusion chromatography. **b,** Fluorescence size exclusion chromatography (FSEC) of rhodamine G hepcidin (RhoG-hepcidin). RhoG-hepcidin co-elutes with nanodisc-FPN and with a nanodisc-FPN:Fab45D8 complex. **c,** RhoG-hepcidin binding to nanodisc-FPN in the presence of 10 µM $CoCl_2$ measured by fluorescence polarization reveals a K_D of 7.7 nM. **d,** Fluorescence polarization of RhoG-hepcidin increases further with Fab45D8, consistent with formation of a larger complex. Importantly, Fab45D8 does not decrease RhoG-hepcidin binding. **e,** RhoG-hepcidin binds to FPN (FPN+hepcidin) but not to Fab45D8 alone (Fab45D8+hepcidin). Order of hepcidin and Fab45D8 addition does not influence the increase in fluorescence polarization for a Fab45D8-FPN-hepcidin complex. **f,** FSEC shows RhoG-hepcidin binding to nanodisc-FPN is competed by excess unlabelled hepcidin used for structural studies.

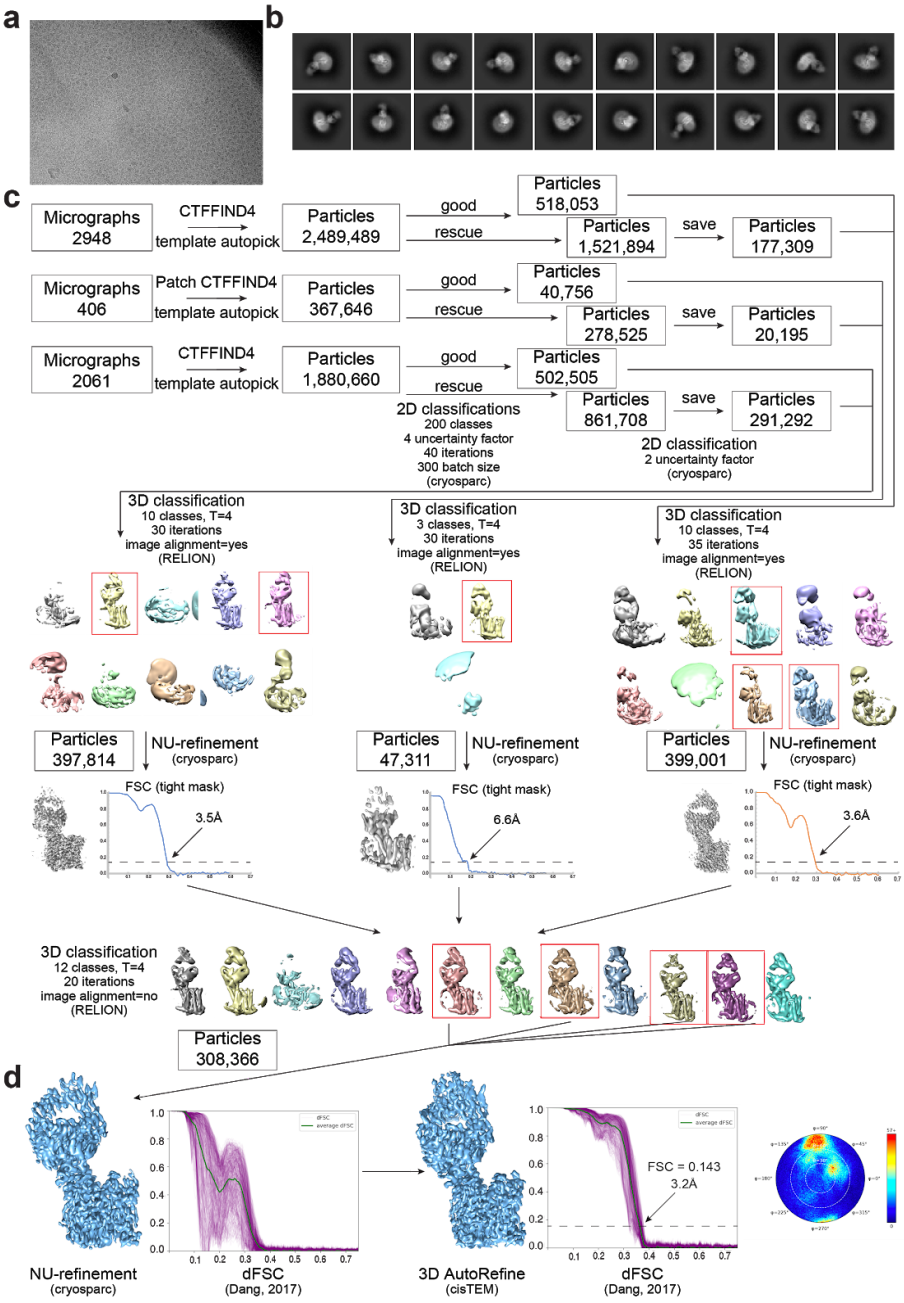

Supplementary Figure 3. Cryo-EM data processing for FPN-Fab45D8. a, Representative motion-corrected micrograph collected on the Titan Krios showing monodisperse FPN-Fab45D8 nanodisc particles. **b,** Examples of “good” 2D class averages that were used in 3D classification. **c,** Flowchart showing image processing pipeline for FPN-Fab45D8. Initial processing, through 2D classification, was performed in cryoSPARC. Particles were then transferred, using csparc2star.py, to RELION for 3D classification, then to cryoSPARC for a nonuniform refinement, and finally to cisTEM for refinement. The number of particles moving into each step are noted. **d,** Final refinements from cryosparc and cisTEM beside their directional FSC curves calculated using dfsc.0.0.1.py. Angular distribution plot from cisTEM is shown.

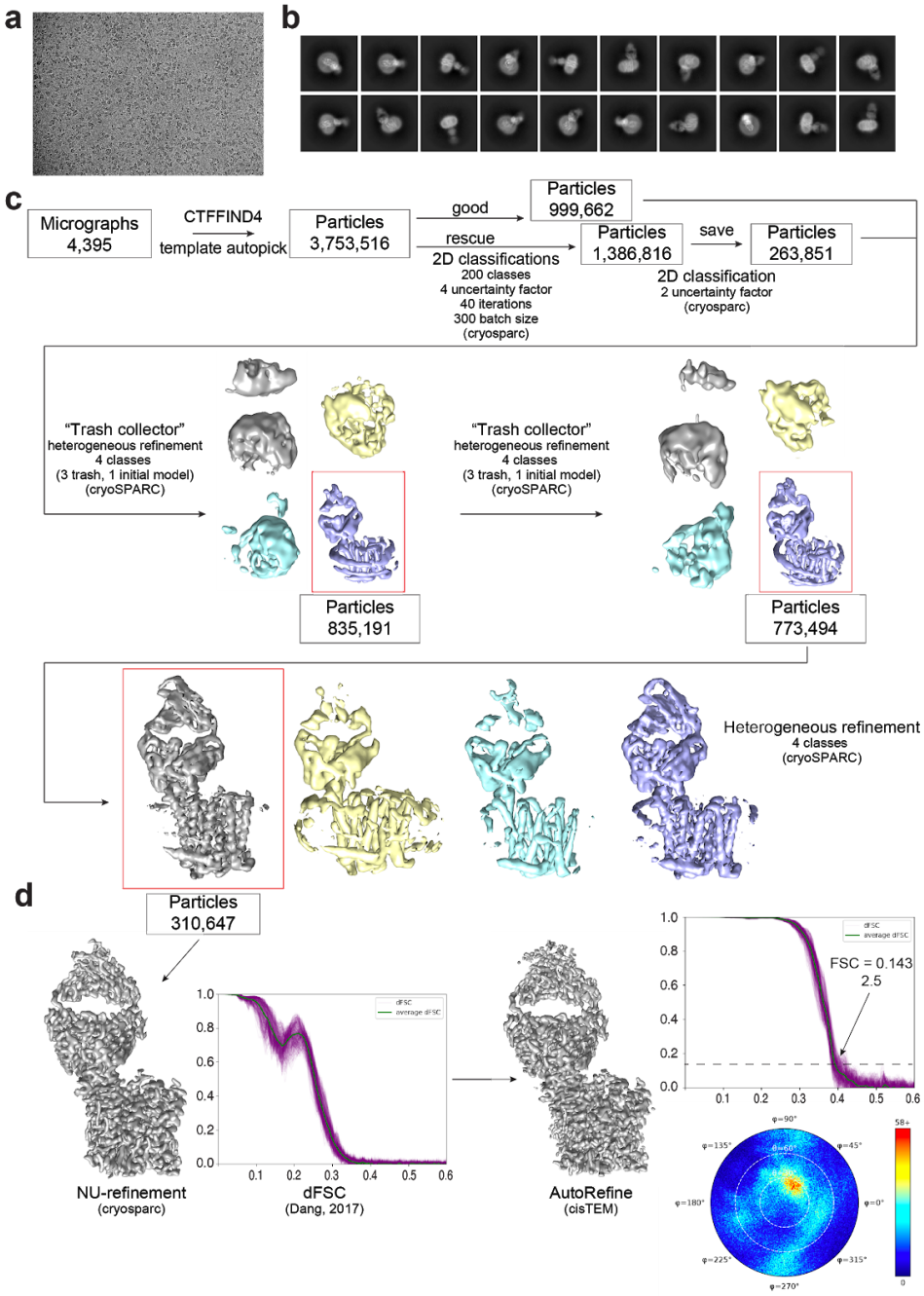

Supplementary Figure 4. Cryo-EM data processing for Co^{2+}-hepcidin-FPN-Fab45D8. a, Representative motion-corrected micrograph collected on the Titan Krios showing monodisperse Co^{2+}-hepcidin-FPN-Fab45D8 nanodisc particles. **b,** Examples of "good" 2D class averages that were used in 3D classification. **c,** Flowchart showing image processing pipeline for Co^{2+}-hepcidinF-PN-Fab45D8. Initial processing, through nonuniform refinement, was performed in cryoSPARC. A final subset of particles were transferred to cisTEM for refinement. The number of particles moving into each step are noted. **d,** Final refinements from cryosparc and cisTEM beside their directional FSC curves calculated using dfsc.0.0.1.py. Angular distribution plot from cisTEM is also shown.

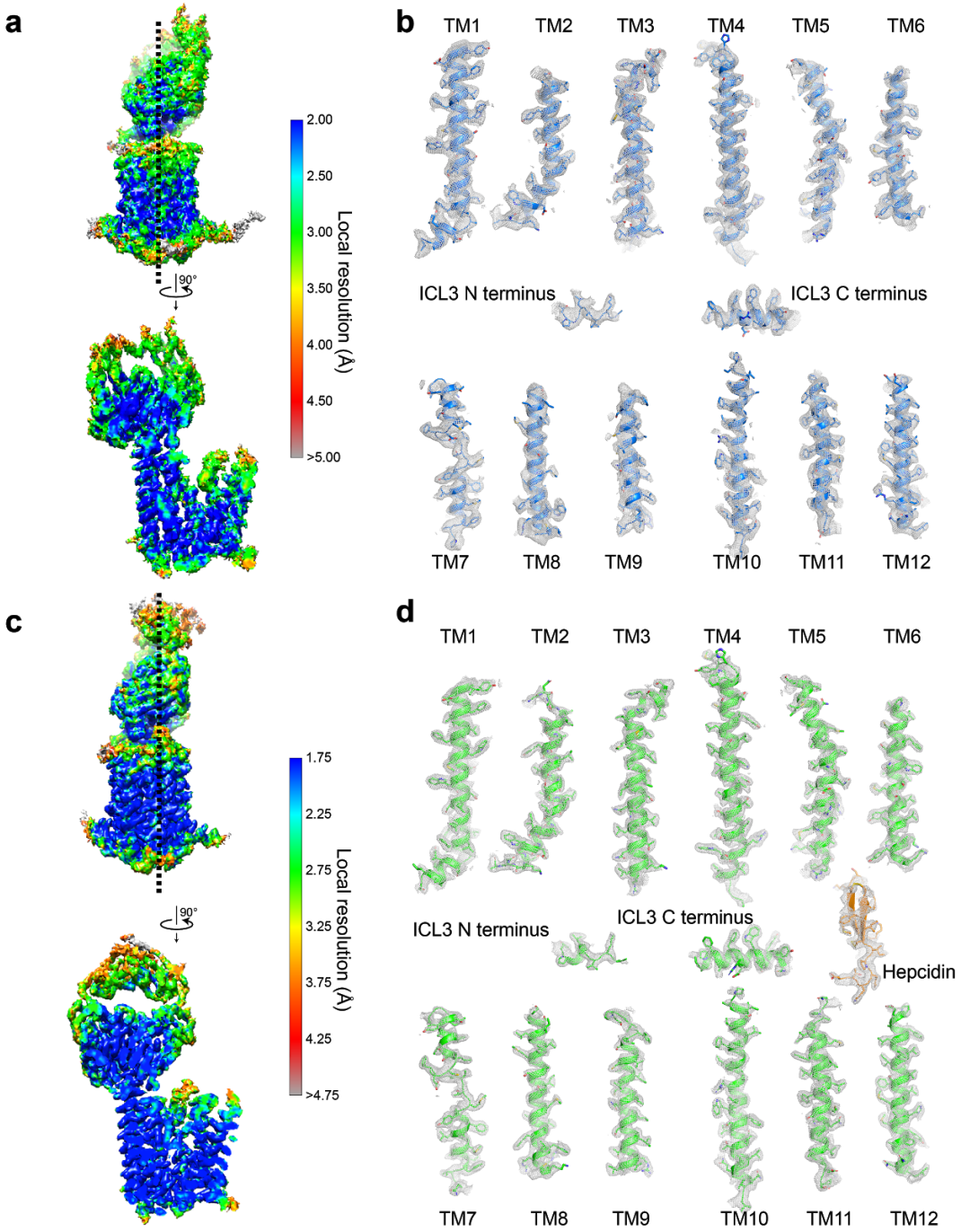

Supplementary Figure 5. Cryo-EM map density for FPN. Local resolution estimation by ResMap for the apo-FPN-Fab45D8 complex (**a**) and for the Co^{2+}-hepcidin-FPN-Fab45D8 complex (**c**). Two views of each complex are shown. Shown in grey mesh is cryo-EM map density for individual FPN transmembrane helices for the apo-FPN-Fab45D8 complex (**b**) and for the Co^{2+}-hepcidin-FPN-Fab45D8 complex (**d**). Mesh depicts density within a 2.5 Å radius of any modeled atom.

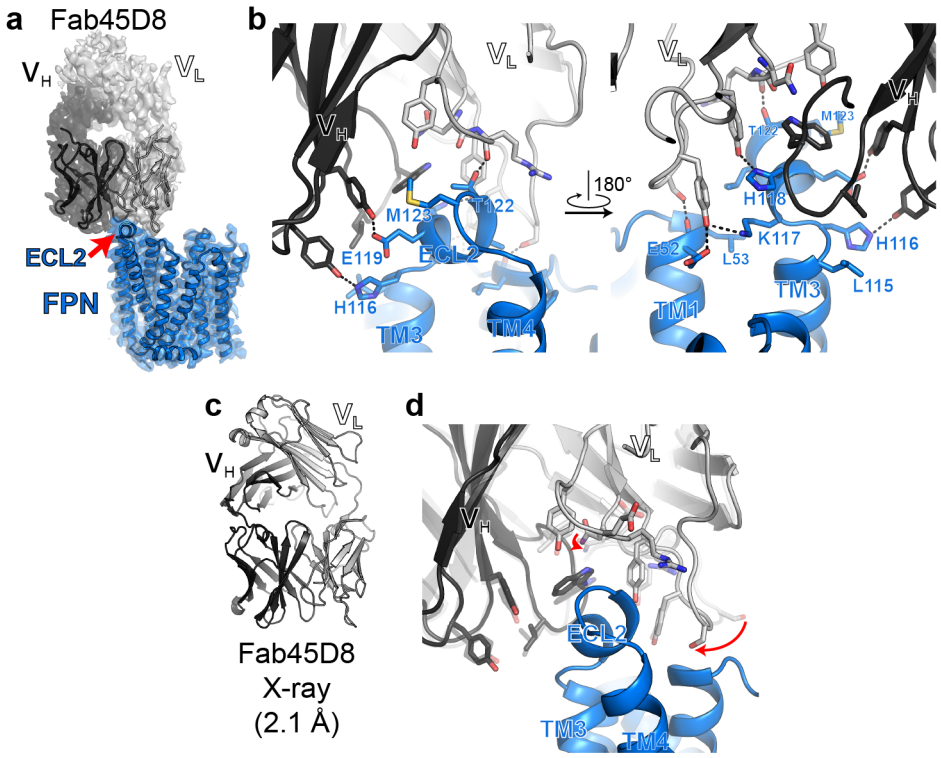

Supplementary Figure 6. Structure of Fab45D8 and interaction with FPN. a, Cryo-EM density of FPN and Fab45D8. Although density is observed for the constant regions of Fab45D8, it is not of sufficient quality to unambiguously model. **b,** Fab45D8 makes extensive contacts with FPN extracellular loop 2 (ECL2) with both the heavy (V_H) and light (V_L) chains. **c,** Crystal structure of Fab45D8 at 2.1 Å. **d,** Comparison of Fab45D8 alone (transparent cartoon and sticks) and bound to FPN. The binding site residues of Fab45D8 change minimally upon binding FPN.

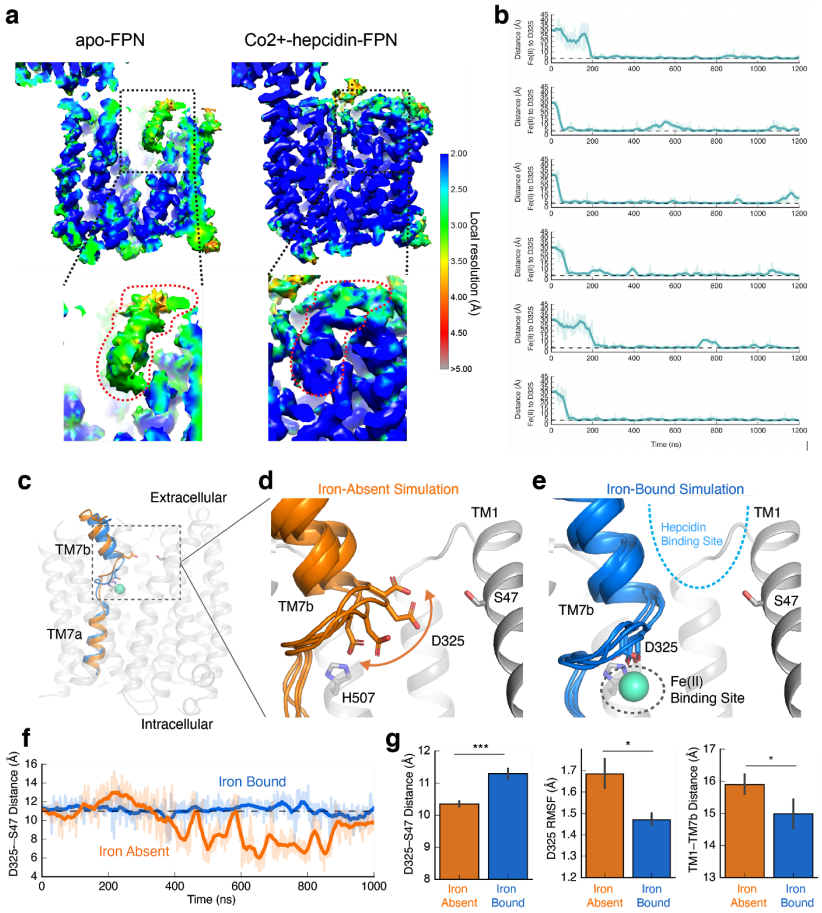

Supplementary Figure 7. Molecular dynamics simulations of iron binding to apo FPN. a, ResMap of FPN cryo-EM density. Insets show local resolution around TM7b. **b,** Each graph corresponds to an independent simulation where Fe^{2+} ions start in solution and bind spontaneously to the proposed iron binding site. Distance shown is from the ion to the nearest oxygen atom of the D325 side chain. Thick traces represent a 15-ns sliding mean and thin traces represent unsmoothed values. Timetraces include 30 ns of equilibration. The average time to bind (the time from start of production simulation to when the measured distance is less) was 71 ns. **c,** Representative conformations of TM7 from simulations with iron bound (blue) or absent (orange). **d,** In the absence of bound iron, D325 is mobile and can move into the cavity between TM7b and TM1. The top of TM7b can also tilt away from TM1. Four representative frames from simulation are overlaid. **e,** In simulations with Fe^{2+} bound, interaction with the ion restricts the mobility of D325 and, in turn, TM7b. **f,** Iron-bound and iron-absent simulations show differences in the dynamics and position of D325, as measured by the distance between D325 Cγ and S47 Cβ. **g,** Comparison of conformation and dynamics with and without iron bound. With iron bound, D325 moves away from TM1 into the iron binding site (left), the root-mean-square fluctuation (RMSF) of D325 decreases (middle), and the extracellular end of TM7b moves closer to TM1 (right). For these comparisons, 6 simulations for each condition were used, each 2.0 μs in length. Error bars are s.e.m. and p-values were calculated using Mann-Whitney U test (* $p<0.05$, *** $p<0.001$).

Supplementary Table 1: Cryo-EM statistics

	FPN-Fab45D8 (EMDB-21539) (PDB 6W4S)	FPN-Co^{2+}-hepcidin-Fab45D8 (EMDB-21599) (PDB 6WBV)
Data collection and processing		
Microscope/Detector	Titan Krios/Gatan K3 with Gatan Bioquantum Energy Filter	Titan Krios/Gatan K3 with Gatan Bioquantum Energy Filter
Imaging software and collection	SerialEM, 3x3 image shift	Serial EM, 3x3 image shift
Magnification	105,000	105,000
Voltage (kV)	300	300
Electron exposure (e–/Å^2)	66	66
Dose rate (e–/pix/sec)	8	8
Frame exposure (e–/Å^2)	0.55	0.55
Defocus range (μm)	-0.8 to -2.0	-0.8 to -2.0
Pixel size (Å)	0.834 (physical)	0.834 (physical)
Micrographs	5,415	4,395
Reconstruction		
Autopicked particles (template-based in cryosparc)	4,737,795	3,753,516
Particles in 3D classification	1,326,130 (RELION)	1,263,513 (cryosparc)
Particles in final refinement	308,386 (cisTEM)	310,647 (cisTEM)
Symmetry imposed	C1	C1
Map sharpening *B* factor (Å^2)	-130	-90
Map resolution, global FSC (Å)		
FSC 0.5, unmasked/masked	7.1/3.4	4.0/2.7
FSC 0.143, unmasked/masked	4.0/3.2	3.3/2.5
Refinement		
Initial model used (PDB code)	5AYN	5AYN, 3H0T
Model resolution (Å)		
FSC 0.5, unmasked/masked	3.6/3.4	3.0/2.8
Model composition		
Non-hydrogen atoms	4968	6869
Protein residues	650	892
B factors (Å^2)		
Protein	67.31	27.30
Ligand	N/A	55.15
Water	N/A	31.32
R.m.s. deviations		
Bond lengths (Å)	0.004	0.006
Bond angles (°)	0.563	0.872
Validation		
MolProbity score	2.31	2.10
Clashscore	7.90	7.10
Poor rotamers (%)	4.45	4.26
EMRinger score	2.37	4.32
CaBLAM score	2.06	0.69
Ramachandran plot		
Favored (%)	94.38	96.47
Allowed (%)	5.62	3.53
Disallowed (%)	0	0

Supplementary Table 2: Fab45D8 crystal structure statistics

	Fab45D8 (PDB 6W4V)
Data collection	
Space group	$P2_1$
Cell dimensions	
a, *b*, *c* (Å)	72.19, 36.43, 84.95
α, β, γ (°)	90.0, 112.26, 90.0
Resolution (Å)	39.31 - 2.09 (2.14 - 2.09)[a]
R_{sym} or R_{merge}	0.087 (1.385)
$I / \sigma I$	7.9 (1.2)
Completeness (%)	99.9 (99.9)
Redundancy	3.3 (3.5)
CC (1/2) (%)	99.6 (30.0)
Refinement	
Resolution (Å)	39.31 - 2.09
No. reflections	24736
R_{work} / R_{free} (%)	21.6 / 24.7
No. atoms	
Protein	3356
Ligand/ion	20
Water	125
B-factors	
Protein	57.87
Ligand/ion	86.17
Water	51.43
R.m.s. deviations	
Bond lengths (Å)	0.01
Bond angles (°)	0.92

[a]Values in parentheses are for highest-resolution shell.

Supplementary Table 3: Molecular dynamics simulations

Condition	Number of Simulations	Duration (μs)	Notes
Iron absent	6	2.2 (each)	No iron was added
Iron bound	6	2.2 (each)	A single Fe^{2+} ion was placed in the proposed binding site initially
Iron in bulk solvent	6	2.2 (each)	15 Fe^{2+} ions were placed randomly in solution initially